Korean J. Chem. Eng., **27**(6), 1773-1779 (2010)
DOI: 10.1007/s11814-010-0385-2

Simulation of methanol-to-olefin reaction over SAPO-34 catalysts with different particle sizes: Formation of active sites and deactivation

Hag Geum Kim*, Kwang Young Lee, Hoi-Gu Jang**, Yo Soon Song**, and Gon Seo**,†**

*Department of Environmental and Chemical Engineering, Seonam University, Namwon, Jeonbuk 590-170, Korea
**School of Applied Chemical Engineering and the Research Institute for Catalysis,
Chonnam National University, Yongbong-dong 300, Gwangju 500-757, Korea
(*Received 12 June 2010 • accepted 21 July 2010*)

Abstract−Conversion profiles of methanol-to-olefin (MTO) reaction over SAPO-34 catalysts with different particle sizes were simulated using two kinetic models. The MTO reaction was assumed to consist of three steps: the formation of hexamethylbenzene (HMB), the production of lower olefins over HMB and the further condensation of HMB to polyaromatic hydrocarbons. To reflect the effect of particle size on the MTO reaction, only the space near the external particle surface was considered to be available for HMB formation in Model I, whereas an effectiveness factor and a deactivation function were introduced in Model II. The simulated conversion profiles of the MTO reaction by both models successfully confirmed the presence of an induction period and deactivation, but Model II showed a better agreement between the experimental and simulated results because of its inclusion of the deactivation function and its consideration for the gradient of methanol concentration.

Key words: MTO Reaction, SAPO-34, Particle Size, Induction Period, Deactivation, Simulation

INTRODUCTION

The methanol-to-olefin (MTO) process successfully produces lower olefins, the most important raw materials of the petrochemical industry, from various non-petroleum sources such as natural gas, coal and biomass [1-3]. The MTO process has thus been considered a promising alternative to the naphtha cracking process which is currently used to produce most of the lower olefins. The UOP/Hydro MTO process over Ni-SAPO-34 catalyst achieves high yield of lower olefins above 90% [4]. Furthermore, the control of reaction conditions and the modification of catalysts provide high flexibility for the product selectivity required to meet the increasing demand of certain olefins.

Although the mechanism of the MTO reaction is very simple, following the pathway of methanol (MeOH)→dimethylether (DME) →lower olefins, various reaction intermediates have been suggested to explain the carbon-carbon bond formation from MeOH. Despite extensive controversy on the nature of the intermediates, an *in situ* solid MAS NMR experiment combined with an on-lined gas chromatograph revealed that the hexamethylbenzene (HMB) molecules formed in the cages of the SAPO-34 molecular sieve act as active sites for the formation of carbon-carbon bonds through the side-chain alkylation and paring reaction of polymethylbenzenes [5-9]. The time required for the formation of HMB in the cages determines the induction period of the MTO reaction, whereas the further condensation of HMB to polyaromatic hydrocarbon (PAH) through alkylation and condensation results in catalyst deactivation.

Several kinetic modeling studies on the MTO reaction have been reported [10-17]. The extent of the reaction over SAPO-34 catalysts was calculated by assuming a simple reaction mechanism consisting of the formation of lower olefins and coke from the intermediates produced from MeOH and DME. Coke deposition was considered an important factor for the catalyst deactivation. The additional consideration for the oligomerization of the produced lower olefins followed by cracking resulted in a good simulation of the olefin composition in the product streams. The coke deposited in cages induced steric hindrance for reactants and products, leading to a high olefin selectivity at the coke deposit level of 5-7 wt%. A detailed kinetic model, including all possible elementary reactions, achieved a good simulation capable of describing even the variation of each lower olefin yield with space velocity.

The kinetic model of the MTO reaction based on the formation and degradation of HMB in SAPO-18 cages appropriately simulated the induction period for the production of lower olefins and the catalyst deactivation with time on stream (TOS) [15-17]. The increase in the yield of lower olefins with lengthening TOS reflected the increase in the HMB concentration in the catalysts, while the decrease in the HMB concentration due to the further condensation of HMB to PAH caused catalyst deactivation. The simulation provided yield profiles of the lower olefins that were highly coincident with the experimental ones. The importance of the temperature effect on the composition of lower olefins in the MTO reaction over the phosphorous-modified ZSM-5 catalyst was confirmed by the simulation based on a hydrocarbon pool mechanism [18].

The MTO reaction over SAPO-34 catalyst exhibited considerable variation in conversion profiles according to the particle size of the catalyst [19-22]. The SAPO-34 catalyst with small particles was very active even at the beginning of the reaction and did not show any induction period, while that with large particles required a definite induction period. Furthermore, the former maintained its catalytic activity for a longer time than the latter did. These differ-

†To whom correspondence should be addressed.
E-mail: gseo@chonnam.ac.kr

ences in the activation and deactivation of SAPO-34 catalysts according to their particle size have been explained by the space limitation that allows the formation of HMB, because the inner space of large particles does not attain a sufficient concentration of MeOH in its cages [20]. The large external surface area of the SAPO-34 catalyst with small particles has many cages that facilitate HMB formation. Therefore, a high HMB loading in the catalysts induces a long catalyst life and a high catalytic activity even at the beginning of the reaction. However, to the best of our knowledge, no paper has quantitatively discussed the effect of particle size on the catalytic activity.

In another aspect, the effect of particle size on MTO reaction over SAPO-34 catalysts can be explained by the difference in their effectiveness factors. Slow diffusion of MeOH into the SAPO-34 catalyst with large particles lowers its effectiveness factor, while that with small particles has a high factor. The deactivation of SAPO-34 catalysts due to the occupation of their cages by PAHs is also dependent on their particle size because this PAH blocking effect is more severe on large particles [22,23]. An exponential function, $\exp(-\alpha_i, t)$ with α_i values that vary according to the particle size of SAPO-34, can be useful in representing its deactivation process [24].

In this paper, we simulate the MTO reaction over SAPO-34 with different particle sizes using two different models to clarify the effect of particle size on their activation and deactivation. The space near the external surface of SAPO-34 is assigned as an available space for the formation of HMB in Model I, but an effectiveness factor and a deactivation function are introduced to simulate the conversion profiles in Model II. The simulation results clearly demonstrate the significant role played by particle size on the progress of the MTO reaction over SAPO-34 catalysts.

MODELING

The MTO reaction over SAPO-34 was assumed to be comprised by three steps, as suggested by Gayabo [15,16]: the formation of HMB from MeOH, the production of lower olefins over HMB, and the further condensation of HMB to PAH as shown below:

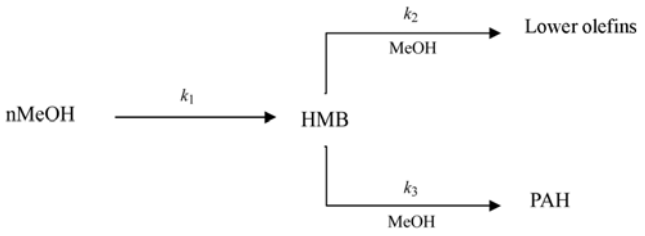

Scheme 1. Reaction pathway of the MTO reaction over SAPO-34 catalysts.

where k_1, k_2 and k_3 are the reaction rate constants for the formation of HMB, for the production of lower olefins and for the further condensation of HMB to PAH, respectively. All three reactions are considered to be irreversible and first order to MeOH because one MeOH molecule is involved in the elementary alkylation steps for the formation of HMB, olefin and PAH [15-17].

1. Model I

Since the cages of the SAPO-34 molecular sieve are connected by small eight membered-ring entrances (3.8×3.8 Å), the occlusion of HMB and PAH in the cages induces a diffusion restriction on the mass transfer of reactants and products. MeOH molecules easily diffuse into the cages near the external surface and produce HMB molecules, while the formation of HMB molecules in the cages distant from the external surfaces is suppressed by the slow diffusion of MeOH molecules. The exclusion of the cages distant from the external surface reduces the number of cages that participate to the MTO reaction. Scheme 2 clearly shows that the unavailable space (gray) for HMB formation in cubic SAPO-34 particles increases with increasing particle size. The SAPO-34 catalyst with small particles has only a small fraction of the unavailable space for HMB formation, while that with large particles has a large unavailable space. The decrease in the allowed space for the formation of HMB causes the long induction period because a sufficient amount of HMB is required for the production of lower olefins. A rapid deactivation of the SAPO-34 catalyst with large particles is also responsible for the small amount of HMB molecules per a given mass of catalyst because the further condensation of HMB to PAH causes the deficiency of HMB molecules in a short time.

The number of cages available for the formation of HMB molecules per gram of cubic SAPO(l_{par}) particles with their side length l_{par}, N_{cage}, can be calculated by Eq. (1) when only the cages at a distance l_{acc} from the external surface participate in the MTO reaction.

$$N_{cage} = \frac{C_{cage}[l_{par}^3 - (l_{par} - 2l_{acc})^3]}{l_{par}^3 \rho} \quad (1)$$

where C_{cage} and ρ denote the concentration of cages per volume and

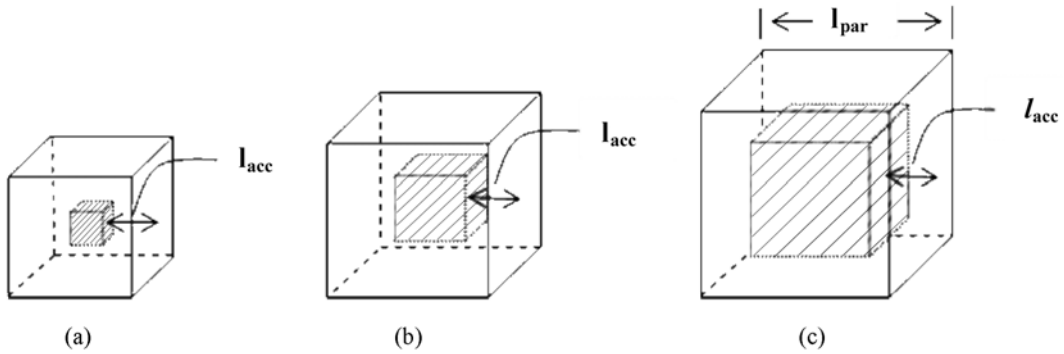

Scheme 2. Variation of the available space (transparent) for the formation of HMB molecules according to the particle size of SAPO-34 catalysts in the MTO reaction.

the density of SAPO(l_{par}), respectively. If the number of cages occluded by HMB and PAH per gram of SAPO(l_{par}) are denoted as N_{HMB} and N_{PAH}, respectively, and C_{MeOH} refers to the concentration of MeOH in the catalyst, the rates for the formation of HMB, for the consumption of MeOH, and for the further condensation of HMB to PAH are expressed by Eqs. (2)-(4).

$$r_{HMB}=k_1[N_{cage}-N_{HMB}-N_{PAH}]C_{MeOH}-k_3N_{HMB}C_{MeOH} \quad (2)$$

$$-r_{MeOH,\,consumed}=12k_1[N_{cage}-N_{HMB}-N_{PAH}]C_{MeOH} + 3k_2N_{HMB}C_{MeOH}+6k_3N_{HMB}C_{MeOH} \quad (3)$$

$$r_{PAH}=k_3N_{HMB}C_{MeOH} \quad (4)$$

The numbers, 12, 3 and 6 in Eq. (3), reflect the numbers of methanol molecules required for the formation of HMB, propylene and the most simple PAH, octamethylnaphthalene, respectively. The term ($k_3N_{HMB}C_{MeOH}$) exhibits the formation rate of lower olefins. Since the selectivity to propylene is considerably high over SAPO-34, propylene is considered as a typical olefin formed in the MTO reaction.

Since $N_{HMB}=N_{PAH}=0$ at the initial condition, the conversion of MeOH in a flow reactor can be calculated by the above equations when l_{acc}, k_1, k_2 and k_3 are given. At a steady state, the production rate of lower olefins on HMB is relatively rapid, compared to the formation rate of HMB and the further condensation rate of HMB to PAH, and, therefore, the conversion of MeOH, X, is given by Eq. (5).

$$X=\frac{(-r_{MeOH,consumed})\cdot m}{r_{MeOH,fed}} \quad (5)$$

where m is the mass of the SAPO(l_{par}) catalyst loaded in the reactor and $r_{MeOH,fed}$ and $-r_{MeOH}$ denote the molar feed rate of MeOH and the calculated rate of MeOH consumed over a gram of catalyst, respectively. If the calculated rate of MeOH consumption is lower than the rate at which it is fed, Eq. (5) facilitates the calculation of MeOH conversion. However, if the calculated rate of MeOH consumption over HMB exceeds the MeOH feed rate, then all the MeOH fed is completely consumed, so X=1.

$$X=\frac{(-r_{MeOH,consumed})\cdot m}{r_{MeOH,fed}},\ \text{if}\ (-r_{MeOH,consumed})\cdot m<r_{MeOH,fed} \quad (6)$$

$$X=1,\ \text{if}\ (-r_{MeOH,consumed})\cdot m>r_{MeOH,fed} \quad (7)$$

Fig. 1 shows the calculated conversion profiles in the MTO reaction over the SAPO-34($l_{par}=7\times10^{-6}$ m) with different k_1, k_2, k_3 and

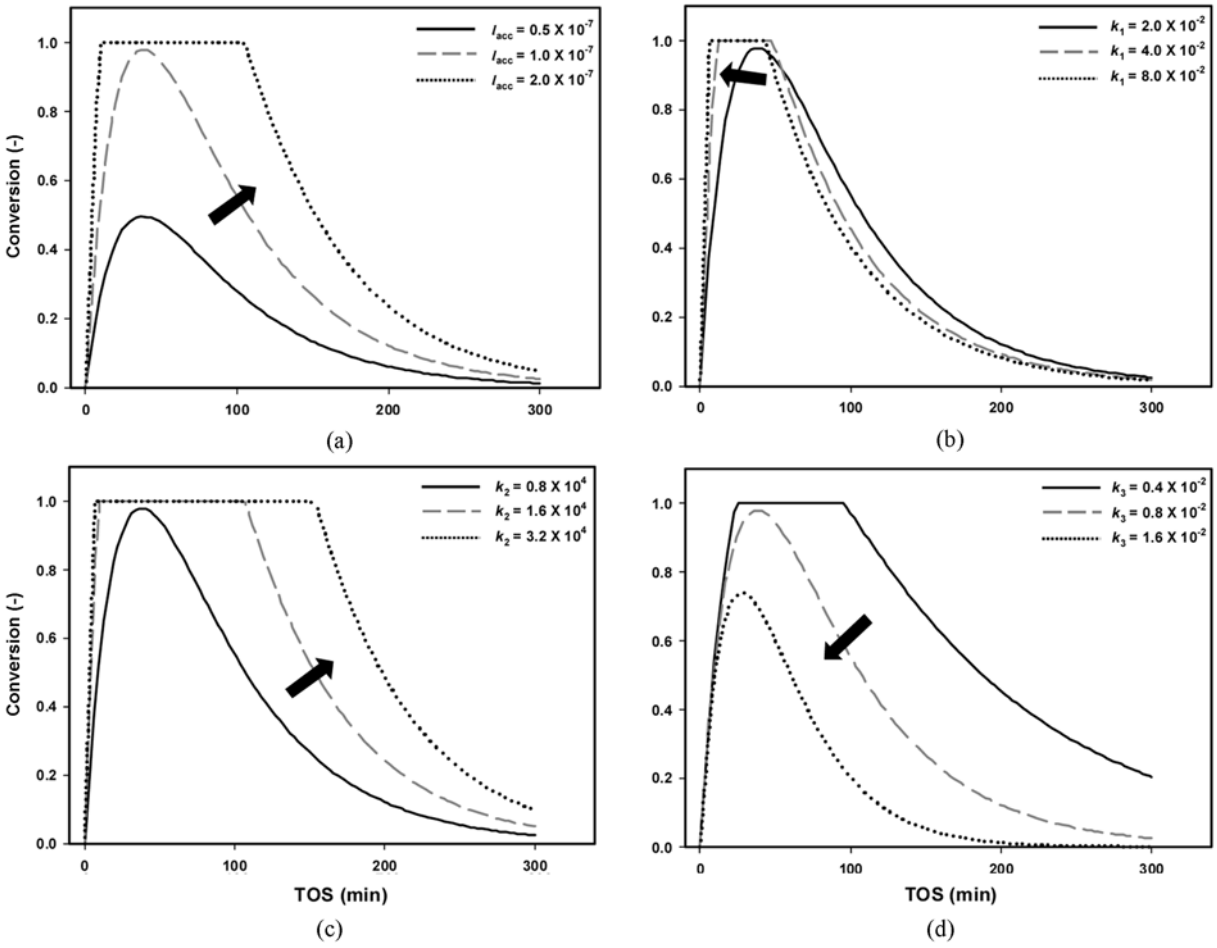

Fig. 1. Calculated conversion profiles over SAPO-34 with l_{par} of 7×10^{-6} m in the MTO reaction as a function of (a) l_{acc}, (b) k_1, (c) k_2, and (d) k_3. The medium values of other parameters used in the simulation, except varied one, were $l_{acc}=1.0\times10^{-7}$ m, $k_1=2.0\times10^{-2}$ min^{-1}, $k_2=0.8\times10^{4}$ min^{-1} and $k_3=0.8\times10^{-2}$ min^{-1}.

l_{acc} values. The effect of l_{acc} on the conversion is represented in Fig. 1(a) when the rate constants, k_1, k_2 and k_3 are given as 2.0×10^{-2} min^{-1}, 0.8×10^{4} min^{-1} and 0.8×10^{-2} min^{-1}, respectively. Since the increase of l_{acc} increases the available space of SAPO-34 for HMB formation, the long l_{acc} results in a rapid increase in the conversion at the beginning of the MTO reaction (rapid activation) and a long catalyst life (slow deactivation). However, the short l_{acc}, i.e., $l_{acc}=0.5\times10^{-7}$ m, induces a slow activation and rapid deactivation due to the reduction of the available space for HMB formation.

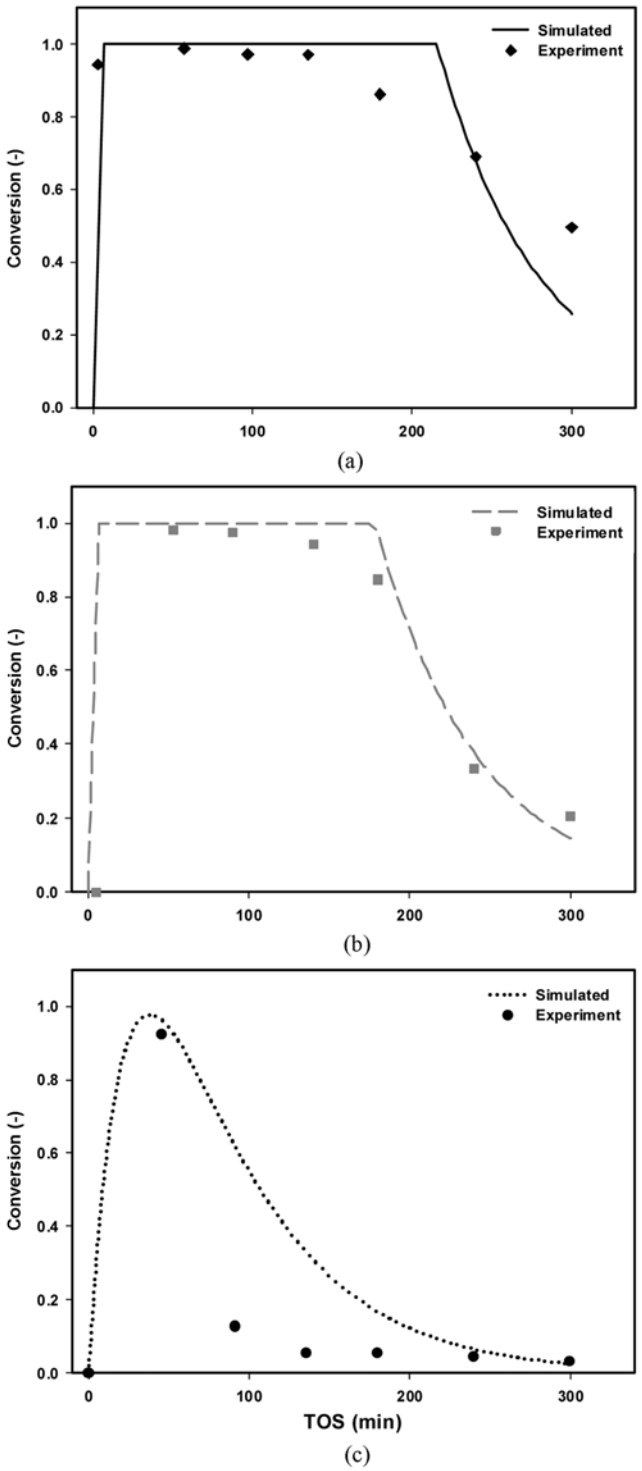

Fig. 2. Simulated conversion profiles over the SAPO-34 catalysts with different particle sizes: (a) $l_{par}=4.0\times10^{-7}$ m, (b) $l_{par}=1.0\times10^{-6}$ m, and (c) $l_{par}=7.0\times10^{-6}$ m. The parameters used in the simulation were $l_{acc}=1.0\times10^{-7}$ m, $k_1=2.0\times10^{-2}$ min^{-1}, $k_2=0.8\times10^{4}$ min^{-1} and $k_3=0.8\times10^{-2}$ min^{-1}.

Since k_1 is the rate constant for HMB formation, the high k_1, as shown in Fig. 1(b), significantly increases the conversion at the beginning. However, this increased conversion also increases N_{PAH} according to Eq. (4), and, therefore, the high k_1 also causes rapid deactivation. Since k_2 governs the formation rate of lower olefins from MeOH on each HMB molecule, it corresponds to the turnover frequency of HMB in the MTO reaction. Fig. 1(c) shows the conversion profiles with different k_2 values. Although the effect of k_2 on the conversion at the beginning is small, the time for complete conversion lengthens at high k_2 because complete conversion is achieved even on a small amount of HMB. The deactivation rate is mainly dependent on k_3, as shown in Fig. 1(d). The initial increasing slopes of the conversion profiles are similar to each other, regardless of k_3, but the increase in k_3 results in severe catalyst deactivation.

Fig. 2 compares the simulated conversion profiles on the SAPO-34 catalysts with different particle sizes. The experimental data were reported in our previous paper [20]. The only effect of the particle size is a considerable variation in conversion profiles, despite l_{acc}, k_1, k_2 and k_3 being maintained constant. The SAPO-34 catalyst with fine particles ($l_{par}=4.0\times10^{-7}$ m) shows a high conversion even at the beginning and a slow deactivation. On the contrary, the initial conversions on the SAPO-34 catalysts with medium ($l_{par}=1.0\times10^{-6}$ m) and coarse ($l_{par}=7.0\times10^{-6}$ m) particles were zero, representing their slow activation due to the small amount of the available space for HMB formation. The SAPO-34 catalyst with small particles has a relatively large number of available cages for the formation of HMB molecules, resulting in a rapid activation and slow deactivation.

Although Model I facilitates the simulation of the variations of the activation and deactivation of SAPO-34 catalysts in the MTO reaction according to their particle size, the simulated conversion profiles at the deactivation step show appreciable differences from those obtained in the experiment. The allowed space for HMB formation is considered to be fixed in Model I, but the movement of the reaction region of SAPO-34 in the MTO reaction to the center of particles with increasing TOS was reported [25]. The considerable discrepancy between the simulated and experimental results at the deactivation step may be responsible for the shift of available space to the center of particles.

2. Model II

Since the cage entrances of SAPO-34 molecular sieve are small, the mass transfer rates of reactants and products through the entrances are important in determining the overall rate of the MTO reaction over it. As a result, the SAPO-34 catalyst with large particles has a lower effectiveness factor than that with small particles. The diffusion limitation in the catalyst becomes more severe at the deactivation step because PAH molecules present in the cages largely suppress the mass transfer. A deactivation function, $\exp(-\alpha_p t)$, is useful to reflect the variation of the deactivation of SAPO-34 with its particle size [24]. The deactivation parameter, α_p, representing the deactivation susceptibility of SAPO-34 due to the cage occupation by PAH, is large for the catalyst with large particles.

The rates for the formation of HMB, for the consumption of MeOH and for the further condensation of HMB to PAH in the MTO reaction followed the pathway described in Scheme 1, and are expressed by the dimensionless fractions (y_i) of MeOH, HMB and PAH, as shown below:

$$r_{HMB}=\eta_j\exp(-\alpha_j, t)[k_1'y_{MeOH}-k_3'y_{HMB}y_{MeOH}] \quad (8)$$

$$-r_{MeOH}=\eta_j\exp(-\alpha_j, t)[12k_1'y_{MeOH}+3k_2'y_{HMB}y_{MeOH}+6k_3'y_{HMB}y_{MeOH}] \quad (9)$$

$$r_{PAH}=\eta_j\exp(-\alpha_j, t)k_3'y_{HMB}y_{MeO} \quad (10)$$

where j refers to the SAPO-34 catalysts with different particle sizes. To discriminate the rate constants from those used in Model I, apostrophes were added, such as k_1', k_2' and k_3'. Although the physical meaning of the rate constants used in Model II is essentially the same as that used in Model I, their values are considerably different from those used in Model I because the concentrations of materials are expressed in fractions in Model II.

Since $y_{HMB}=0$ at the initial condition and y_{MeOH} is constant throughout the catalyst, the conversion of MeOH can be calculated by Eqs. (8)-(10) following the same procedure used in Model I, when η_j, α_j, k_1', k_2' and k_3' are given. The effectiveness factors for three SAPO-34 catalysts with different particle sizes are set as 1.0, 0.5 and 0.1 to exhibit the relative effect of particle size on their catalytic perfor-

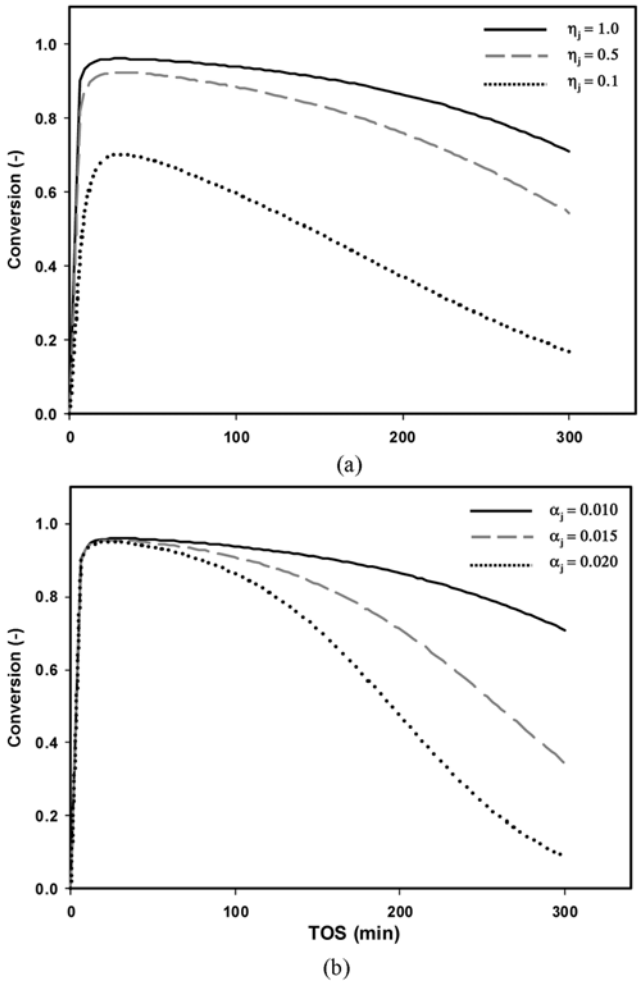

Fig. 3. Calculated conversion profiles over SAPO-34 as a function of (a) effectiveness factor and (b) deactivation parameter. For the simulation α_j=0.01 for (a) and η_j=1 for (b). k_1', k_2' and k_3' were 12.5 min^{-1}, 25 min^{-1} and 0.125 min^{-1}, respectively.

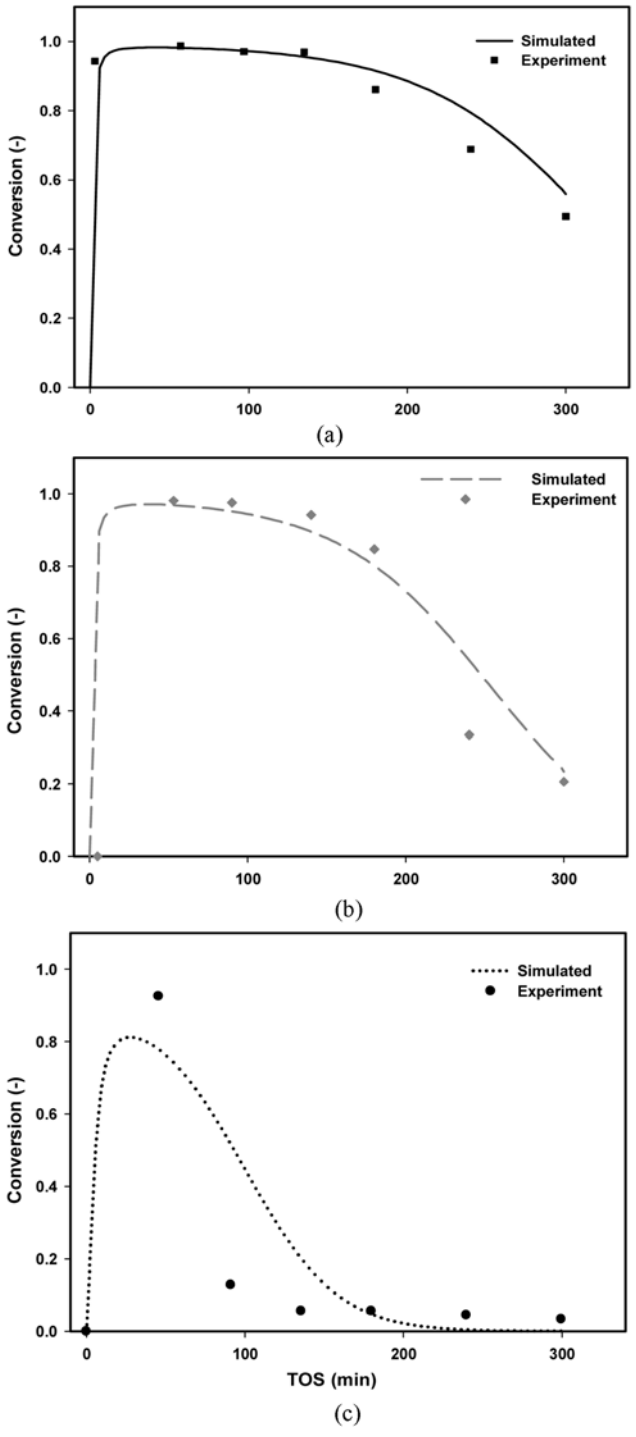

Fig. 4. Simulated conversion profiles over the SAPO-34 catalysts with different particle sizes: (a) $l_{par}=4.0\times10^{-7}$ m, (b) $l_{par}=1.0\times10^{-6}$ m, and (c). In the simulation, $l_{par}=7.0\times10^{-6}$ m, and α_j and η_j were set as 1 and 0.01 for (a), 0.8 and 0.012 for (b) and 0.114 and 0.02 for (c), respectively. The same k_1', k_2' and k_3' were used in the simulation as to be 12.5 min^{-1}, 25 min^{-1} and 0.125 min^{-1}, respectively.

mance according to the increase in their particle size. The deactivation parameters of the SAPO-34 catalysts are obtained from the best plots as 0.010, 0.015 and 0.020, with the increasing particle size. Although the variation of k_1', k_2' and k_3' induces considerable changes in the simulated conversion profiles, the trends in the changes according to the rate constants are similar to those observed in Fig. 1 because the reaction scheme of Model II is completely the same as that of Model I. Therefore, the variations of conversion profiles with the rate constants are not shown here in order to prevent unnecessary repetition.

Fig. 3 shows the calculated conversion profiles with varying η_j and α_j. The reduction of η_j causes the overall decrease of the conversion throughout TOS, while the increase of α_j increases the decreasing slope of the conversion profiles only at the deactivation step. Since the effectiveness factor affects the catalyst performance, the lower effectiveness factors reduce the conversion profiles over the complete range. However, the deactivation function only influences the deactivation step. The change in α_j does not affect the conversion profiles at the beginning, but the increase in α_j rapidly decreases the conversion at the deactivation step.

The effectiveness factor and deactivation parameter of SAPO-34 are varied according to the particle size. The SAPO-34 catalyst with small particles has a high effectiveness factor and a low deactivation parameter, but that with large particles has a low effectiveness factor and a high deactivation parameter. Fig. 4 shows the simulated conversion profiles in the MTO reaction over the SAPO-34 catalysts with different particle sizes using Model II. The simulated conversion profiles, especially on the SAPO-34 catalysts with medium and coarse particles, show excellent agreement with the experimental results from the beginning all the way to the deactivation step.

DISCUSSION

The MTO reaction over the SAPO-34 catalysts with different particle sizes can be simulated by using both Models I and II based on the reaction scheme considering HMB as an active intermediate. The formation of HMB induces an induction period and the further condensation of HMB to PAH results in catalyst deactivation. The rate constants for the formation of HMB, for the production of lower olefins and for the further condensation determine the conversion profiles. However, the available space for HMB formation must be limited in Model I to simulate the experimental ones, while an effectiveness factor and a deactivation function are necessary in Model II. Although the simulated conversion profiles are in good accord with the experimental ones, the coincidence at the deactivation step is not good in Model I. The simple loss of HMB due to the further condensation to PAH is insufficient to describe the deactivation step because the inner space of the large particles becomes useful for HMB formation at later TOS. The introduction of the deactivation function, $\exp(-\alpha_j t)$, in Model II is very effective in simulating the deactivation step. The long diffusion paths of the reactants and products in large particles require high values of α_j to simulate rapid deactivation.

ACKNOWLEDGEMENTS

This work was supported by the Priority Research Centers Program through the National Research Foundation of Korea (NRF) funded by the Ministry of Eduaction, Science and Technology (2010-0094056).

NOMENCLATURE

C_{cage} : cage concentration in SAPO-34 [mol/m^3]
C_{MeOH} : MeOH concentration in SAPO-34 [mol/m^3]
k_1, k_1' : rate constant for HMB formation [mol/m^3/min, 1/min]
k_2, k_2' : rate constant for lower olefin production [mol/m^3/min, 1/min]
k_3, k_3' : rate constant for the further condensation of HMB to PAH [mol/m^3/min, 1/min]
l_{acc} : length for reactant access [m]
l_{par} : catalyst particle size [m]
m : catalyst mass [g]
N_{cage} : number of cages in SAPO-34 [mol/g]
N_{HMB} : number of HMB in SAPO-34 [mol/g]
N_{PAH} : number of PAH in SAPO-34 [mol/g]
r_{HMB} : rate of HMB formation [mol/min]
$-r_{MeOH}$: rate of MeOH consumption [mol/min]
r_{PAH} : rate of PAH formation [mol/min]
$r_{MeOH,fed}$: rate of MeOH fed [mol/min]
y_{MeOH} : fraction of MeOH [-]
y_{HMB} : fraction of HMB [-]
y_{PAH} : fraction of PAH [-]
X : conversion [-]
ρ : density of SAPO-34 [g/m^3]
η_j : effectiveness factor of catalyst j [-]
α_j : deactivation parameter of catalyst j [-]

REFERENCES

1. C. D. Chang, *Catal. Rev. Sci. Eng.*, **25**, 1 (1983).
2. M. Stocker, *Micropor. Mesopor. Mater.*, **29**, 3 (1999).
3. F. J. Keil, *Micropor. Mesopor. Mater.*, **29**, 49 (1999).
4. J. Q. Chen, A. Bozzano, B. Glover, T. Fuglerud and S. Kvisle, *Catal. Today*, **106**, 103 (2005).
5. J. F. Haw, W. Song, D. M. Marcus and J. B. Nicholas, *ACC. Chem. Res.*, **36**, 317 (2003).
6. J. F. Haw and D. M. Marcus, *Top. Catal.*, **34**, 317 (2005).
7. M. Hunger, M. Seiler and A. Buchholz, *Catal. Lett.*, **74**, 61 (2001).
8. Y. Jiang, J. Huang, V. R. R. Marthala, Y. S. Ooi, J. Weitkamp and M. Hunger, *Micropor. Mesopor. Mater.*, **105**, 132 (2007).
9. G. Seo and B. G. Min, *Korean Chem. Eng. Res.*, **44**, 329 (2006).
10. A. G. Gayubo, A. T. Aguayo, A. E. Sánchez del Campo, A. M. Tarío and J. Bilbao, *Ind. Eng. Chem. Res.*, **39**, 292 (2000).
11. D. Chen, H. P. Rebo, A. Grønvold, K. Moljord and A. Holmen, *Micropor. Mesopor. Mater.*, **35-36**, 121 (2000).
12. S. Soundararajan, A. K. Dalai and F. Berruti, *Fuel*, **80**, 1187 (2001).
13. T. Y. Park and G. F. Froment, *Ind. Eng. Chem. Res.*, **40**, 4172 (2001).
14. T. Y. Park and G. F. Froment, *Ind. Eng. Chem. Res.*, **40**, 4187 (2001).
15. A. G. Gayubo, R. Vivanco, A. Alonso, B. Valle and A. T. Aguayo, *Ind. Eng. Chem. Res.*, **44**, 6605 (2005).
16. A. T. Aguayo, A. G. Gayubo, R. Vivanco, A. Alonso and J. Bilbao, *Ind. Eng. Chem. Res.*, **44**, 7279 (2005).
17. A. G. Gayubo, A. T. Aguayo, A. Alonso and J. Bilbao, *Ind. Eng.*

Chem. Res., **46**, 1981 (2007).
18. M. Kaarsholm, B. Rafii, F. Joensen, R. Cenni, J. Chaouki and G. S. Patience, *Ind. Eng. Chem. Res.*, **49**, 29 (2010).
19. Y. H. Song, H. J. Chae, K. E. Jeong, C. U. Kim, C. H. Shin and S. Y. Jeong, *J. Korean Ind. Eng. Chem.*, **19**, 559 (2008).
20. K. Y. Lee, H. J. Chae, S. Y. Jeong and G. Seo, *Appl. Catal. A: Gen.*, **369**, 60 (2009).
21. D. Chen, K. Moljord, T. Fuglerud and A. Holmen, *Micropor. Mesopor. Mater.*, **29**, 191 (1999).
22. N. Nishiyama, M. Kawaguchi, Y. Hirota, D. V. Vu, Y. Egashira and K. Ueyama, *Appl. Catal. A: Gen.*, **362**, 193 (2009).
23. J. W. Park, J. Y. Lee, K. S. Kim, S. B. Hong and G. Seo, *Appl. Catal. A: Gen.*, **339**, 36 (2008).
24. H. S. Fogler, *Elements of Chemical Reaction Engineering*, Prentice Hall International Series, New Jersey, USA (2006).
25. D. Mores, E. Stavitski, M. H. F. Kox, J. Kornatowski, U. Olsbye and B. M. Weckhuysen, *Chem. Eur. J.*, **14**, 11320 (2008).